Ordered Microphase Separation in Thin Films of PMMA−PBA Synthesized by RAFT: Effect of Block Polydispersity

Wilasinee Sriprom,[†] Michael James,[‡,§] Sébastien Perrier,[†] and Chiara Neto*[,†]

School of Chemistry and Key Centre for Polymers & Colloids, The University of Sydney, NSW 2006, Australia; School of Chemistry, The University of Sydney, NSW 2006, Australia; and Bragg Institute, Australian Nuclear Science and Technology Organisation (ANSTO), PMB 1, Menai, NSW 2234, Australia

Received November 24, 2008; Revised Manuscript Received March 5, 2009

ABSTRACT: The microphase separation of diblock copolymers synthesized by reversible addition−fragmentation chain transfer (RAFT) polymerization, containing one monodisperse block (poly(methyl methacrylate), PMMA) and one polydisperse block (poly(butyl acrylate), PBA), was investigated in thin films (<100 nm). The formation of ordered microphase-separated domains was observed by atomic force microscopy (AFM) and resulted in four morphologies, depending on composition and film thickness: parallel lamellae, hexagonally packed perforated lamellae (PL), parallel cylinders ($C_{||}$), and hexagonally packed spheres, and in $C_{||}$-to-PL-to-$C_{||}$ transitions. Polydispersity of the PBA block shifts the phase boundaries toward higher PBA volume fraction values with respect to those expected for monodisperse block copolymers and stabilizes the perforated lamella morphology. Neutron reflectivity data confirmed that lamellae parallel to the substrate form at a very low PBA volume fraction, $f_{PBA} = 0.23$. Polydispersity of the PBA block also has the effect of stabilizing each microphase domain over a film thickness regime larger than expected for monodisperse blocks. For the first time RAFT-polymerized block copolymers are shown to microphase separate with high reproducibility and with excellent degree of order, hence proving to be ideal systems to test the effect of polydispersity on microphase separation.

Introduction

In the past few decades, block copolymers have attracted increasing attention in a range of technological areas such as microelectronics, nanotechnology, and nanofabrication. In particular, thin films of diblock copolymers have recently received great attention for their potential of producing templates for large area patterned surfaces in various nanofabrication applications, such as suboptical lithographic masks, nanoporous films, nanoparticle synthesis, nanomaterial templating, photonic materials, and high-density magnetic recording devices (for recent reviews see refs 1−3). Such a wide range of applications is due to the tunability of size, shape, and composition of the molecules and their ability to self-assemble into several different ordered nanodomains. Additionally, block copolymers are becoming more commercially interesting as more economical and simpler synthetic routes emerge, producing versatile materials with improved mechanical properties over standard polymeric materials.

Diblock copolymers are macromolecules composed of two chemically different polymers covalently bonded. If the two blocks are incompatible, upon annealing they spontaneously self-assemble into a range of well-defined and ordered microphase-separated morphologies that are tens of nanometers in size.[4−14] This arrangement is determined by the balance between the enthalpic gain of demixing of the two blocks and the entropic cost of chain confinement within domains. The microphase behavior of diblock copolymers depends on the volume fraction of the blocks, f, and on the degree of incompatibility, χN, where N is the overall degree of polymerization (number of monomers in the chain) and χ is the Flory−Huggins interaction parameter. For strongly incompatible A−B monodisperse copolymers, the microphase separation morphology changes from lamellae for volume fraction $f_A \approx 0.30-0.60$ to hexagonally packed cylinders of B in a matrix of A for $f_A \approx 0.65$ to spheres of B in a matrix of A for $f_A \approx 0.90$.[5] More complicated nanostructures, such as perforated lamellae, gyroid structures, and double-diamond morphologies, have also been observed when the copolymer composition falls within a narrow range between the cylindrical and lamellar morphologies but have been suggested to be metastable.[4,15−17]

In thin films of diblock copolymers, microphase separation is also strongly affected by the wetting properties of each block at the substrate surface and at the air/film interface.[2,18] In copolymers that form lamellae parallel to the substrate, a multilayered structure is formed, where the film thickness is quantized in terms of the bulk lamellar period, L_0.[19] When one block prefers both the substrate and the air interfaces (i.e., symmetric wetting), the film is smooth if its thickness t is equal to $t = nL_0$, where n is an integer. Conversely, when one block prefers the substrate and the other block prefers the air interface (i.e., asymmetric wetting), smooth films are attained if the film thickness is $t = (n + {}^1/_2)L_0$.[6−8,13,14,20,21] If the thickness of the prepared film is not commensurable with L_0, islands or holes with a step height of L_0 form on the top surface. This topography allows the preferred block(s) to be present at both interfaces and also to maintain the characteristic period throughout the whole film thickness. The occurrence of the hole/island morphology has been observed often for lamellar domains and also for cylinder-forming[22,23] and sphere-forming[9,24] systems. In a few studies on thin films of cylinder-forming block copolymers, domain transitions between cylinders oriented parallel to the substrate ($C_{||}$) and a perforated lamella (PL) have been observed at particular film thicknesses and surface fields.[22,25−27]

Most studies involving thin block copolymer films have investigated the behavior of "ideal" systems, namely copolymers in which blocks were both strongly segregated due to their different chemical properties and monodisperse in molecular weight due to the particular synthetic route employed. This focus on ideal systems was justified by the assumption that a strong

* To whom correspondence should be addressed: e-mail c.neto@chem.usyd.edu.au; Ph +61-2- 9351 2752; Fax +61-2- 9351 3329.
[†] School of Chemistry and Key Centre for Polymers & Colloids, The University of Sydney.
[‡] School of Chemistry, The University of Sydney.
[§] Australian Nuclear Science and Technology Organisation.

10.1021/ma9004428 CCC: $40.75
Published on Web 03/26/2009

segregation of blocks and a narrow molecular weight distribution were necessary to achieve a high degree of ordering.[28] However, neither of these conditions is stringent. Recent experiments[29,30] and theoretical studies[28,31−36] have shown that some well-ordered morphologies can be achieved even with relatively polydisperse blocks. This is of strong practical interest since some synthetic techniques, which provide a certain level of polydispersity, have proven economical and therefore more attractive to the manufacturing industry. Studying phase separation in copolymers made of partially compatible blocks is furthermore useful, as partially compatible blocks can be synthesized in the absence of solvent (via bulk polymerization), thus making the synthetic process easier and more environmentally friendly and might open new applications for block copolymer systems.

In this study, we address both these issues by investigating, for the first time, the microphase separation of block copolymers of poly(methyl methacrylate) (PMMA)−poly(*n*-butyl acrylate) (PBA) synthesized by reversible addition−fragmentation chain transfer (RAFT) polymerization. Most block copolymers investigated in the past two decades were synthesized by anionic polymerization, which requires specific reaction conditions, including the use of completely dry, highly pure reagents, and inert atmospheres.[37] Our approach instead is to use living radical polymerization (LRP) techniques, which have become in the past decade simple and valid alternatives for large-scale applications in polymer chemistry because of the ease with which control over molecular weight, polydispersity, and molecular architectures can be achieved.[38,39] Among the available LRP systems, RAFT polymerization is one of the most versatile processes because a large variety of monomers with different functionalities can be polymerized under standard reaction conditions, producing a wide range of polymeric architectures.[40−43] RAFT polymerization is based on the introduction of a small amount of dithioester in a conventional free-radical system consisting of monomer and initiator. The transfer of the chain transfer agent (CTA) between growing radical chains and dormant polymeric chains regulates the growth of the molecular weight and limits the termination reactions.[44,45] Termination reactions are unavoidable, producing a small amount of so-called "dead" chains, which in turn may increase the polydispersity over the value PDI = 1.05 typical of anionic polymerization.

In this study, we used RAFT polymerization to synthesize four block copolymers of fixed overall degree of polymerization N, while changing the relative volume fraction of the PMMA and PBA blocks. By studying several block copolymers with different volume fraction but nearly constant χN, we effectively take a horizontal slice through the phase diagram of this system. The particular block copolymer system investigated here, PMMA−PBA, has rarely been studied in the literature, partially because of the chemical similarity of the two blocks. The few published studies on PMMA−PBA block copolymers mainly focused on the synthesis of the copolymers by atom transfer radical polymerization (ATRP) or anionic polymerization and on their characterization by calorimetry.[46−51] Noncontact atomic force microscopy (AFM) has been often used to characterize block copolymer microphase separation,[22,24−26,52−58] but we are aware of only two studies by Tong et al.[49,50] that investigated monodisperse PMMA−PBA−PMMA copolymers by AFM and in thick films. Small-angle X-ray scattering studies on bulk samples of polydisperse PMMA−PBA di- and triblock copolymers by Ruzette et al. found that morphology boundaries are shifted with respect to those observed in ideal monodisperse block copolymers as a result of unbalanced polydispersity between the two blocks.[51] In this study we employ AFM in noncontact mode, which allows us, using phase contrast, to map the lateral distribution of each block near the film surface due to the different mechanical properties of the PMMA (glassy) and PBA (soft) blocks. AFM is particularly suited to the study of phase separation of PMMA−PBA copolymers because staining agents used in transmission electron microscopy (TEM) or elemental signatures in X-ray photoelectron spectroscopy (XPS) are not effective when the two blocks are chemically very similar. Neutron reflectivity was also employed to confirm the microphase separation into domains. Here we discuss the influence of copolymer composition, film thickness, and block polydispersity on the formation of the domains in thin films (<100 nm) of PMMA−PBA.

Table 1. Polymerization Conditions and Monomer Conversion for the Synthesized Polymers

sample		CPDB/MMA/AIBN molar ratio	time (min)	monomer conversion (%)[d]
PMMA28.8K		1/500/0.25	360	55
PMMA15.8K		1/700/0.15[b]	120	17
PMMA50.5K		1/700/0.15[b]	503	73
copolymer[a]	PMMA block	PMMA/BA/AIBN molar ratio		
$PMMA_{40}-PBA_{60}$	PMMA28.8K	1/1000/0.2	180	44
$PMMA_{69}-PBA_{31}$	PMMA28.8K	1/300/0.2[c]	240	44
$PMMA_{21}-PBA_{79}$	PMMA15.8K	1/1000/0.2	360	54
$PMMA_{77}-PBA_{23}$	PMMA50.5K	1/1000/0.2	67	16

[a] The name of each block copolymer reflects the vol % of each block, determined by ^{1}H NMR. [b] Carried out in 15% w/w toluene. [c] Carried out in 40% w/w toluene. [d] Determined by ^{1}H NMR.

Experimental Section

1. Materials. All solvents, monomers, and other reagents were purchased from Aldrich at the highest purity available. Methyl methacrylate (MMA, 99+%) and *n*-butyl acrylate (BA, 99+%) were filtered before utilization through a basic alumina (Brockmann I) column to remove the radical inhibitor. Azobis(isobutyronitrile) (AIBN, 99%) was recrystallized twice from ethanol. 2-(2-Cyanopropyl)dithiobenzoate (CPDB) was synthesized following a published procedure.[59] Air- and moisture-sensitive compounds were manipulated using standard Schlenk techniques under a nitrogen atmosphere.

2. Synthesis and Characterization of Block Copolymers. *2.1. Typical Homopolymerization Procedure: Polymerization of Methyl Methacrylate (MMA) by the RAFT Process−PMMA-28.8K.* MMA (from which inhibitor was previously removed by filtration through activated basic alumina) (15 g, 150 mmol), CPDB (0.0664 g, 0.300 mmol), AIBN (0.0123 g, 0.075 mmol), and toluene (6.4623 g, 30 wt %) were mixed. The oxygen was removed from the reaction mixtures by pumping nitrogen gas into the mixture for 5 min, while allowing the oxygen to be released through an escape needle. The sealed tubes were then heated to 70 °C and removed after 360 min. Reactions were quenched in ice, and the PMMA final product was isolated by precipitation in cold methanol. Conversions (55%) were calculated via ^{1}H NMR, and molecular weight distributions (M_n = 28 800 g/mol, PDI = 1.09) were analyzed via GPC.

2.2. Typical Block Copolymerization Procedure: Block Copolymerization of MMA and n-Butyl Acrylate (BA)−$PMMA_{40}$−PBA_{60}. Poly(methyl methacrylate) (PMMA) homopolymer (28 800 g/mol, PDI = 1.09) was used as macro-chain-transfer agent for the block copolymerization with BA (1000 BA (1.4998 g, 11.7 mmol):1 PMMA (0.3370 g, 0.0117 mmol):0.2 AIBN (0.0004 g, 0.0023 mmol); 30 wt % toluene (0.7875 g at 70 °C for 90 min) following a similar experimental setup as that described above. After precipitation in cold methanol, PMMA−PBA block copolymer (M_n = 77 300 g/mol, PDI = 1.37, 44% conversion of BA) was analyzed by ^{1}H NMR and GPC to characterize the composition and molecular weight distribution.

PMMA block were synthesized by using RAFT polymerization under conditions shown in Table 1. PMMA with M_n = 15 800, 28 800, and 50 500 g/mol hereafter are indicated with PMMA15.8K,

Table 2. Characterization of the Synthesized Polymers

	PMMA−PBA						
sample[a]	M_n (kg/mol)[b]	$PDI_{PMMA-PBA}$[c]	PDI_{PMMA}[c]	PDI_{PBA}[d]	PBA (vol %)[e]	T_g^{PMMA} (°C)	T_g^{PBA} (°C)
$PMMA_{77}-PBA_{23}$	50.5−13.6	1.13	1.08	1.32	23	115	−52
$PMMA_{69}-PBA_{31}$	28.8−11.9	1.29	1.09	1.76	31	111	−47
$PMMA_{40}-PBA_{60}$	28.8−39.7	1.37	1.09	1.57	60	113	−47
$PMMA_{21}-PBA_{79}$	15.8−54.4	1.27	1.15	1.31	79	109	−48

[a] The name of each block copolymer reflects the vol % of each block. [b] Determined by ^{1}H NMR. [c] Determined by THF GPC. [d] Estimated from the PDI values of PMMA and of PMMA−PBA. [e] Based on mass densities at 25 °C of 1.08 and 1.19 g/cm^3 for PBA and PMMA, respectively.

PMMA28.8K, and PMMA50.5K, respectively. A series of PMMA homopolymers were used as the macro-chain-transfer agent (CTA) for the addition of BA monomer to form the second block. A similar experimental setup as that described above was undertaken for this second step under conditions shown in Table 1.

The number-average molecular weight (M_n) and polydispersity index (PDI = M_w/M_n) of the synthesized polymers were determined using size exclusion chromatography (SEC) equipped with a LC 1120 HPLC pump (Polymer Laboratories, UK), a MIDAS (type 830) autosampler (Spark Holland, Netherlands), a differential refractive index (DRI) detector (Shodex, RI-101), a 5.0 mm bead-size guard column (50 × 7.5 mm), and two PLgel 5.0 mm MIXED-C columns (300 × 7.5 mm) in series (Polymer Laboratories, UK). THF was used as the eluent at a flow rate of 1 mL min^{-1} at ambient temperature, and toluene was used as a flow rate marker. Since an organic solvent is used as a mobile phase, the name gel permeation chromatography (GPC) is used. The GPC system was calibrated with poly(methyl methacrylate) (PMMA) standards (Polymer Laboratories, UK), with molecular weights ranging from 690 to 1 944 000 g mol^{-1}. The percentage of monomer that polymerized (monomer conversion) was calculated via ^{1}H NMR.

^{1}H (400 MHz) nuclear magnetic resonance (NMR) spectroscopy was used to determine copolymers compositions and molecular weights. ^{1}H NMR spectra of the polymer products were recorded on a Bruker 400 UltraShield spectrometer at 25 °C using d-chloroform ($CDCl_3$) and tetramethylsilane (TMS) as a solvent and an internal reference, respectively.

3. Thermal Properties Analysis. Thermal properties of the block copolymers were studied by differential scanning calorimetry (DSC) using a TA Instruments DSC 2920 modulated DSC under a nitrogen atmosphere (60 cm^3 min^{-1}). For measurement of the glass transition temperature (T_g), about 5−10 mg samples were heated in an aluminum holder from room temperature (25 °C) to 200 °C, then cooled to −90 °C, and reheated to 200 °C. The heating and cooling rate was set to 10 °C min^{-1}. An empty aluminum pan was used as reference. The T_g value was determined as the midpoint between the onset and the end of a step transition using the TA Instruments Universal Analysis 2000 software.

Thermal stability of the block copolymers were investigated by using a TA Instruments Hi-Res TGA 2950 thermogravimetric analyzer under a nitrogen atmosphere (60 cm^3 min^{-1}). The samples (5−10 mg) were heated from room temperature to 590 °C at a rate of 10 °C min^{-1}. The TA Instruments Universal Analysis 2000 software was used to calculate the onset, the end decomposition temperature, and the residual mass. All of the samples were dried under vacuum at 40 °C for 24 h prior to TGA measurements.

4. Sample Preparation and Atomic Force Microscopy (AFM) Imaging. The surface morphologies of the block copolymer films were characterized with a PicoSPM II AFM (Molecular Imaging, Santa Clara, CA) in noncontact mode at ambient atmosphere. The probes used were NT-MDT NSG10 rectangular cantilevers with a resonant frequency of 190−325 kHz and nominal spring constant of 5.5−22.5 N/m. The observed surface structures were analyzed by WSxM 4.0 Develop 11.3 scanning probe microscopy software.

The precipitated block copolymers were dissolved in toluene to produce ca. 3−10 mg/mL solutions. The dilute solutions of the copolymers were spin coated (Laurell Technologies Corp.) on cleaned silicon wafer substrates, which are coated with a native layer of silicon oxide of thickness 1.8 ± 0.1 nm. The wafers were thoroughly cleaned in order to eliminate chemical and particulate contaminants, by treatment with ultrasound for a few minutes in ethanol and acetone, and then blown dry with a nitrogen jet, inside a laminar flow cabinet.[60] The copolymer films were dried at room temperature overnight to remove the residual solvent and then annealed in a vacuum oven at 180 °C for 16 h prior to AFM observations. The film thickness before annealing (in the following named t) was determined by spectroscopic ellipsometry (Woollam M-2000).

5. Neutron Reflectometry. Neutron reflectivity data were measured on the $PMMA_{77}-PBA_{23}$ film using the Platypus time-of-flight neutron reflectometer and a cold neutron spectrum (3.0 Å ≤ λ ≤ 18.0 Å) at the OPAL 20 MW research reactor (Australian Nuclear Science and Technology Organisation, Sydney).[61] 23 Hz neutron pulses were generated using a disk chopper system (EADS Astrium GmbH) in the medium resolution mode ($\Delta\lambda/\lambda = 4\%$) and recorded on a 2-dimensional helium-3 neutron detector (Denex GmbH). Reflected beam spectra were collected at 0.5° for 2 h (0.3 mm slits) and 2.0° for 6 h (1.2 mm slits). Direct beam measurements were collected under the same collimation conditions for 1 h each.

Structural parameters associated with layers within the PMMA−PBA film were refined using the MOTOFIT package[62] with reflectivity data as a function of momentum transfer normal to the surface Q_z (= $4\pi(\sin\theta)/\lambda$). A structural model was prepared using estimated values of neutron scattering length density (SLD) (Table S1), based on a mass density for the PMMA component of the film of 1.19 and 1.08 g/cm^3 for PBA. The Levenberg−Marquardt method was used to minimize χ^2 values.

Results and Discussion

1. Synthesis of Block Copolymers. Dithiobenzoates are thermally stable chain transfer agents[63] that provide excellent control over the RAFT polymerization of most vinyl monomers. CPDB[59] is a well-documented RAFT agent that has been shown to efficiently control the polymerization of methacrylate and acrylate derivatives and was therefore the chain transfer agent of choice for this study.[44,45] Three PMMA blocks with different molecular weight were synthesized via CPDB-mediated RAFT polymerization and chain extended with BA monomers to form PMMA−PBA block copolymers. The overall degree of polymerization N was kept constant around 600 for all block copolymers except $PMMA_{69}-PBA_{31}$ where $N = 400$. Keeping the block copolymer overall N constant allows us to study the phase diagram of this block copolymer while keeping the product χN constant. By synthesizing several block copolymers with different volume fraction but nearly constant χN, we are effectively taking a horizontal slice through the phase diagram of this system. The number-average molecular weight (M_n), PDI, and chain composition of the synthesized PMMA−PBA block copolymers are listed in Table 2.

Figure 1 shows the GPC traces of $PMMA_{69}-PBA_{31}$ and $PMMA_{40}-PBA_{60}$ compared with that of PMMA28.8K. The monomodal and symmetrical shape of the peak of PMMA28.8K shows good control over the polymerization process, which produced a relatively narrow molecular weight distribution (PDI = 1.08−1.15; see Table 2). A characteristic shoulder on the peak of $PMMA_{69}-PBA_{31}$ at low retention time indicates the occurrence of chain branching during acrylate polymerization,

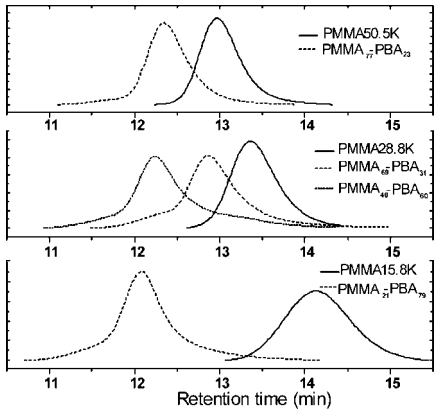

Figure 1. GPC traces of synthesized PMMA block and PMMA−PBA block copolymers. PMMA with M_n = 15 800, 28 800, and 50 500 g/mol are indicated with PMMA15.8K, PMMA28.8K, and PMMA50.5K, respectively. The acronyms of the PMMA−PBA block copolymers include the volume percentage of each block.

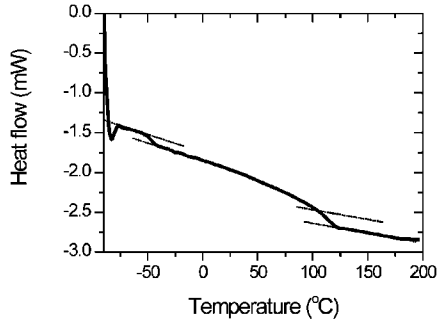

Figure 2. Typical DSC analysis of PMMA−PBA block copolymers. The graph presents heat flow vs temperature data, showing the glass transition of each block forming the $PMMA_{69}$−PBA_{31} block copolymer.

which produces a small proportion of high molecular weight chains.[64] The tail at short retention times on the peaks indicates the presence of a small amount of PMMA "dead" chains in the block copolymers caused by the unavoidable termination reactions of PMMA chains during RAFT polymerization. Successful block copolymerization was demonstrated by a shift to higher molecular weights (shorter retention time) of the peak of the block copolymer when compared to the peak of the PMMA block. Similar results were observed for $PMMA_{77}$−PBA_{23} and $PMMA_{21}$−PBA_{79} (Figure 1).

2. Characterization of Block Copolymers. *2.1. Thermal Properties.* Figure 2 shows the DSC curve of $PMMA_{69}$−PBA_{31}. The graph presents two steps in the baseline of the recorded DSC signal at 112 and −19 °C, indicative of the presence of two glass transition temperatures (T_g) in the block copolymer. The presence of two T_gs is indicative of two microphases in the sample: a hard PMMA region (high T_g) and a soft region corresponding to the PBA block (low T_g). The T_g values of each block vary slightly with molecular weight, as shown in Table 2. Similar DSC data were obtained for all block copolymers (data not shown).

Phase separation of two incompatible blocks in a block copolymer is expected to depend on thermal or solvent annealing. When the block polymer films are annealed above the T_g of the two blocks, the increase in chain mobility allows microphase separation to occur. Films prepared in these studies were annealed for 16 h at 180 °C in a vacuum oven. Thermogravimetric analysis (TGA) indicated that the block copolymers degrade between 350 and 450 °C, which is in agreement with previous observations,[65] thus confirming that

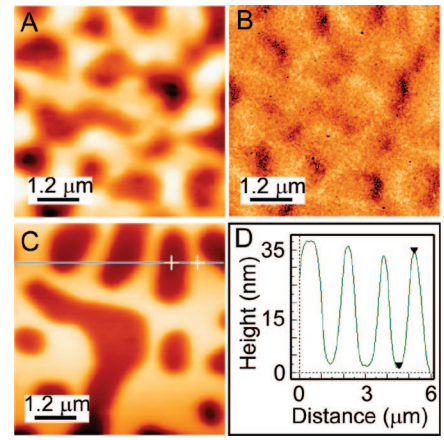

Figure 3. Typical AFM images of thin films of PMMA−PBA block copolymers after thermal annealing. (A) Topography image of a $PMMA_{77}$−PBA_{23} film of preannealing thickness t = 68.8 ± 0.6 nm. (B) Phase image of the same area as in (A). (C) Topography image of a $PMMA_{69}$−PBA_{31} film of preannealing thickness 49.9 ± 0.1 nm. The hole/island morphology characteristic of incomplete lamellae parallel to the substrate is visible. (D) Cross-sectional profile of the topography along the line shown in (C). The peak-to-through height difference is 35 nm. No phase contrast is visible, accounting for the presence of only one block (PBA) at the air/polymer interface. The vertical scale bar is 50 nm in (A) and 70 nm in (C).

the block copolymers are not degraded during annealing. Furthermore, it was shown by AFM analysis that longer annealing times and higher temperature did not substantially change the observed microphase separation (data not shown). This suggests that a minimum in energy (either primary or secondary) was reached after 16 h at 180 °C.

2.2. Investigation of Microphase Separation. Nonannealed spin-cast films of the synthesized block copolymers show a relatively flat and featureless surface, as expected for a disordered phase formed during spin-coating. Upon thermal annealing, the two blocks microphase separate into domains, whose morphology depends on film thickness and copolymer composition.

2.2.1. $PMMA_{77}$−PBA_{23}. $PMMA_{77}$−PBA_{23} contains a volume fraction of PBA f_{PBA} = 0.23. The AFM topography image of an annealed $PMMA_{77}$−PBA_{23} film of initial preannealing thickness t = 69 nm is shown in Figure 3A. For thicknesses between 48 and 61 nm, flat films form upon annealing (data not shown but summarized in Figure 7F). The average surface rms roughness over an area of 5 μm × 5 μm of these films is 1.5 ± 0.5 nm. When t reaches 65 nm, the surface of the film is disturbed by oscillations in film thickness resembling the morphology of spinodal decomposition. However, no preferred oscillation period can be extracted by performing a fast Fourier transformation of the image.

Upon further increasing t to 69 nm, a clear hole/island morphology is formed as shown in Figure 3A. Measurements of the height difference between the bottom of the holes and the top of the islands in the cross-sectional profiles of several AFM topography images (such as the one shown in Figure 3D) reveal that the average step height of the formed holes and islands is 29 ± 2 nm. This height difference between hole and island corresponds to the characteristic lamellar period L_0 for this block copolymer. The corresponding AFM phase images of these films show no phase contrast (Figure 3B), which suggests that the $PMMA_{77}$−PBA_{23} blocks microphase separate in lamellae lying parallel to the silicon substrate ($L_{||}$). The more polar PMMA block preferentially wets the polar silicon wafer substrate,[20] whereas the PBA block tends to segregate to the air interface because of its lower surface energy (ca. 31 mN/m vs ca. 41 mN/m for PMMA).[25,26,56] In all the studied films, a

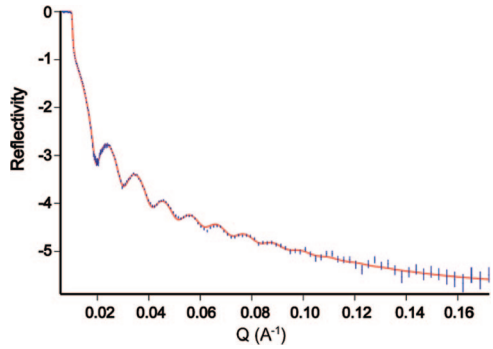

Figure 4. Observed (blue points) and fitted (red line) neutron reflectivity data for a $PMMA_{77}-PBA_{23}$ thin film (57.6 nm). The refined structural model is based on a four-layer lamellar structure with alternating PMMA and PBA layers.

half-lamella (brush) of thickness $b = L_0/2$ is present on the surface of the silicon wafer, as illustrated in Figure 7E. For $PMMA_{77}-PBA_{23}$, a lamellar structure is formed on top of this half-lamella, as depicted in Figure 7A, and the hole/island morphology appears because the film thickness $t \neq (n + {}^1/_2)L_0$. As expected, the hole/island morphology is observed for a film thickness which is larger than the first lamella (hereafter referred to as L1) but smaller than second lamellar (L2), i.e. for L1 < t < L2.

For this block copolymer, a complete L1 is formed when t is in the range of 48−61 nm, and an incomplete L2 is formed for larger t. As shown in Figure 7F, for $t = 85 \pm 6$ nm, flat films are again formed, indicating the formation of a complete L2. Interestingly, for all the prepared films of $PMMA_{77}-PBA_{23}$, a range of film thicknesses can accommodate a complete flat lamella; i.e., a flat film with no hole/island morphology occurs for $t = [(n + {}^1/_2)L_0 \pm$ ca. 15 nm], with $n \geq 1$. This effect is not usually observed in monodisperse block copolymers and is probably due to the relatively large polydispersity of the synthesized PBA block in this copolymer.

The lamellar microphase separation was confirmed by neutron reflectivity data. Figure 4 shows neutron reflectivity data (blue points), and the solid red line shows the calculated reflectivity based upon the refined structural model. Preliminary Fourier transforms of the reflectivity data prior to detailed modeling suggested an overall film thickness of 57 nm, which was used to constrain initial refinement attempts with complex multilayer models.

Various models were used to refine the structure of the PMMA−PBA film using these neutron reflectivity data. A single-layer model of constant composition led to a poor fit to the observed data. A three-layer model with PBA sandwiched between PMMA layers adjacent to the Si substrate and the surface of the film was also modeled and led to a reasonable fit to the observed data ($\chi^2 = 0.0024$).

By far the best fit to the observed neutron data (Figure 4) was obtained by a four-layer polymer model ($\chi^2 = 0.0014$) (Table S2). The difference between scattering lengths of the two polymers meant that we could arrive at a clear four-layer structural model for this film. The overall polymer film thickness was found to be 57.6 nm, comprised of discrete layers of PMMA (20.2 nm) adjacent to the silicon substrate, 16.2 nm of PBA above that, a further layer of PMMA (15.7 nm), and a top layer of PBA (5.5 nm).

2.2.2. $PMMA_{69}-PBA_{31}$. $PMMA_{69}-PBA_{31}$ contains a volume fraction of PBA $f_{PBA} = 0.31$. The microphase separation of $PMMA_{69}-PBA_{31}$ is very similar to that observed for $PMMA_{77}-PBA_{23}$, as shown in Figure 3C. Upon annealing films of thickness 50−58 nm, the characteristic hole/island morphology appears on the surface of the film. The corresponding AFM phase images of these films show no phase contrast, indicating again the formation of asymmetric lamellae lying parallel to the silicon substrate ($L_{||}$). As shown in Figure 3D, the average step height of the formed holes and islands is 36 ± 1 nm, which corresponds to the characteristic lamellar period L_0 for this block copolymer. Here too, as with $PMMA_{77}-PBA_{23}$, the silicon wafer is coated with a whole half-lamella of thickness ${}^1/_2L_0$. As expected, the hole/island morphology is observed for a film thickness ${}^1/_2L_0 < t <$ L1 + ${}^1/_2L_0$, and a flat surface is observed when the film thickness is $t = 63 \pm 4$ nm, indicating the formation of the complete L1. For larger t, islands with a height of L_0 are observed, indicating the formation of an incomplete second lamella (L2).

2.2.3. $PMMA_{40}-PBA_{60}$. $PMMA_{40}-PBA_{60}$ contains a volume fraction of PBA of $f_{PBA} = 0.6$. Figure 5 shows AFM phase and topography images of $PMMA_{40}-PBA_{60}$ annealed films with various initial film thicknesses. Upon annealing, 30 nm-thick films show the formation of hole/island morphology with phase contrast visible on top of the islands, as shown in Figure 5A. The appearance of phase contrast indicates the presence of both PMMA and PBA blocks at the air/film interface within the islands. No phase contrast is visible on the bottom surface, and we interpret this surface as a half-lamellar layer (or brush) formed on the substrate surface with the PMMA block in contact with the silicon oxide.[25,26,56] On top of the islands the phase contrast consists of bright stripes within a dark matrix and a few dark dots on the edge of the islands.

Considering the volume fraction of PMMA in the sample ($f_{PMMA} = 0.4$), the stripe pattern on top of the islands is attributed to PMMA cylinders aligned parallel to the substrate ($C_{||}$), as depicted in Figure 7B. Throughout our study the PMMA blocks appear in the AFM phase images as the blocks with bright phase contrast on the darker PBA blocks. This assignment is confirmed by the relative proportion of bright and dark areas as the polymer composition varies. Phase contrast in noncontact AFM can be reversed by changing imaging parameters,[66] and therefore we kept the scanning parameters as consistent as possible throughout the study.

For films of initial (preannealing) thickness of ca. 30 nm, an incomplete first layer of parallel cylinders (hereafter indicated with $C_{||,1}$) forms on top of the brush. In this case the measured average island thickness is $D = 48 \pm 5$ nm. When the film thickness is increased, the surface area occupied by the islands increases, as expected, showing similar phase contrast as in thinner films, as shown in Figure 5B and insets. The formation of hole/island morphologies with parallel cylinders stacked on top of a brush has been observed before, for thin films of thickness not commensurable with the thickness $t = (nD + b)$, where b is the thickness of the half-lamella adsorbed on the substrate, as shown in Figure 7E.[25]

The cylinder-to-cylinder distance (D_0), estimated as the average distance between the centers of adjacent PMMA bright cylinders in several phase images of different film thickness, was found to be $D_0 = 51 \pm 2$ nm. As shown in Figure 7E, the length D and D_0 are related by the expression $D = (\sqrt{3}/2)D_0$, and our two experimentally measured values for D and D_0 agree with this expression within experimental error.

Structural defects in the $C_{||}$ domain, such as ends of cylinders, visible as dark dots, and three-armed connections between cylinders are present inside the islands in Figure 5A,B. These connections are perhaps precursors of the perforated lamella domain, which becomes dominant in thicker films. This was also previously observed in monodisperse block copolymers, and it is no surprise because the perforated lamella can be considered to be a regular network of three-armed branching points.[67]

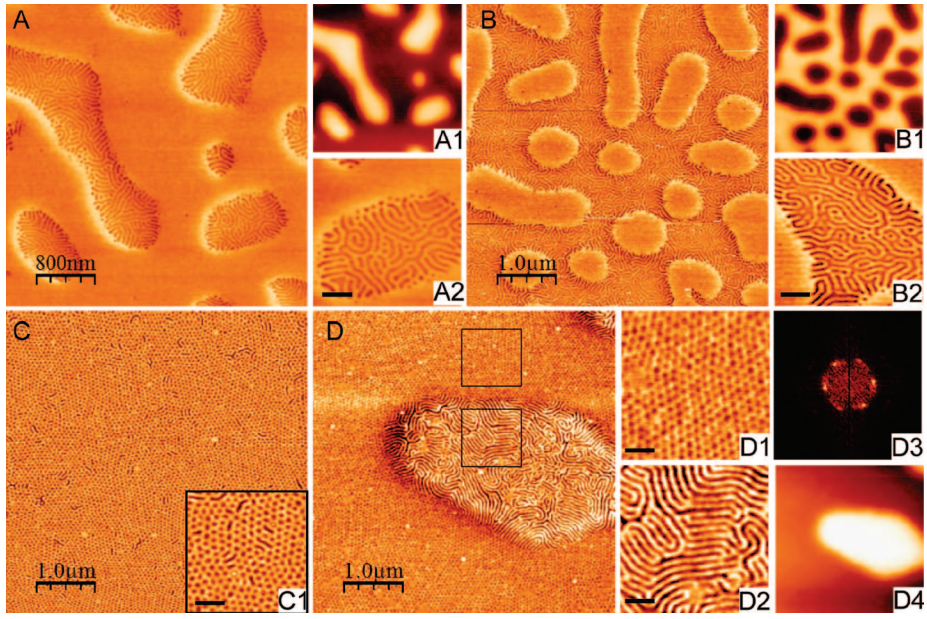

Figure 5. AFM phase images of $PMMA_{40}$−PBA_{60} annealed films with initial film thicknesses of (A) 30.1 ± 0.3, (B) 41.8 ± 0.4, (C) 51.0 ± 0.2, and (D) 68.8 ± 0.5 nm. A1, B1, and D4 are topography images relative to (A), (B), and (D), respectively. A2, B2, C1, D1, and D2 are zoomed images of (A), (B), (C), and (D), respectively. D3 is a fast Fourier transform image of D1. The vertical scale is 70 nm in all the topographical images. The scale bar in all the inset phase images is 200 nm.

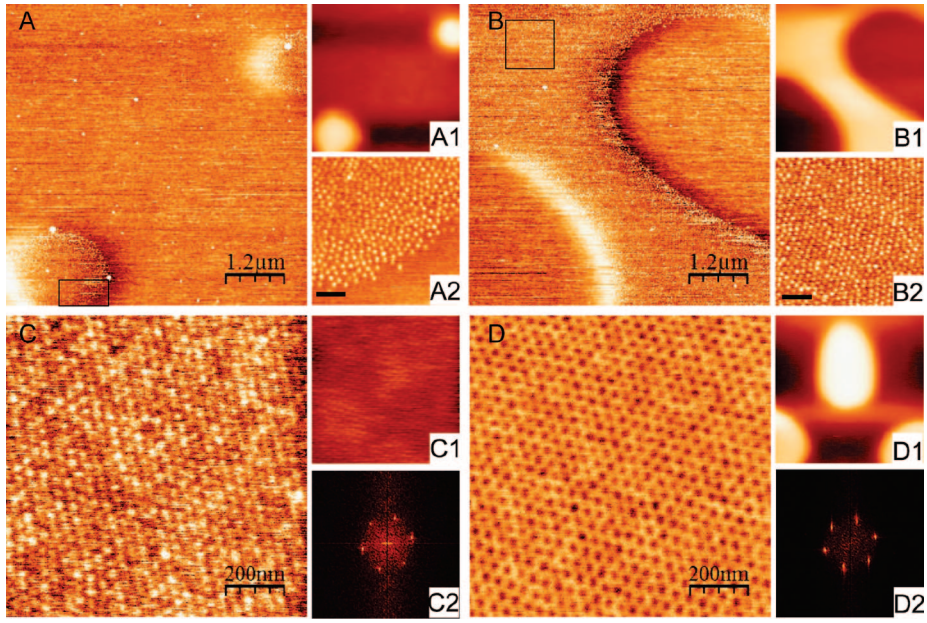

Figure 6. AFM phase images of $PMMA_{21}$−PBA_{79} annealed films with various initial film thicknesses of (A) 20.0 ± 0.3, (B) 33.2 ± 0.4, (C) 54.7 ± 0.3, and (D) 62.1 ± 0.5 nm. (D) is a phase image of the square shown in D1. A1, B1, C1, and D1 are topography image of sample (A), (B), (C), and (D), respectively. A2 and B2 are the zoomed images of (A) and (B), respectively. C2 and D2 are FFT images of (C) and (D), respectively. The vertical scale in A1, B1, and D1 is 70 nm and in C1 is 5 nm. Scale bar in A2 and B2 is 200 nm.

At a film thickness of about 55 ± 4 nm, the parallel cylinders all but disappear, and instead a regular array of dark dots in a bright matrix covers the whole surface, as shown in Figure 5C. Similarly to previously observed patterns,[25,26,67,68] we identify this pattern of hexagonally ordered dark dots as a PMMA lamella (PL) perforated by channels of PBA. For these films, the film thickness is an exact multiple of the closest cylindrical layer thickness plus a brush (as represented in Figure 7B,E). The phase contrast in Figure 5C and inset shows the ordered arrangement of PBA channels inside the perforated PMMA lamella, with only small patches of the parallel cylinders. The amount of isolated parallel PMMA cylinders is reduced to zero by slightly increasing film thickness. The PBA pores in the perforated lamella are arranged in a regular hexagonal array, as shown in the inset 5D1 and in the regular hexagonal display of maxima in the fast Fourier transform (FFT) image in inset 5D3. We can safely say that the perforated lamella is made of PMMA and the channels are made of PBA, based on the phase contrast at the edge of the islands in thicker films, like the one shown in Figure 5D. Here, the phase contrast shows clearly that the PMMA cylinders, which are bright on top of the island, merge into the PL in the film, while the PBA blocks, which are dark on top of the island, turn into channels (pores) inside the PL.

The period of the hexagonal array of pores derived from inset 5D3 is 57 ± 2 nm, a distance slightly larger than the PMMA

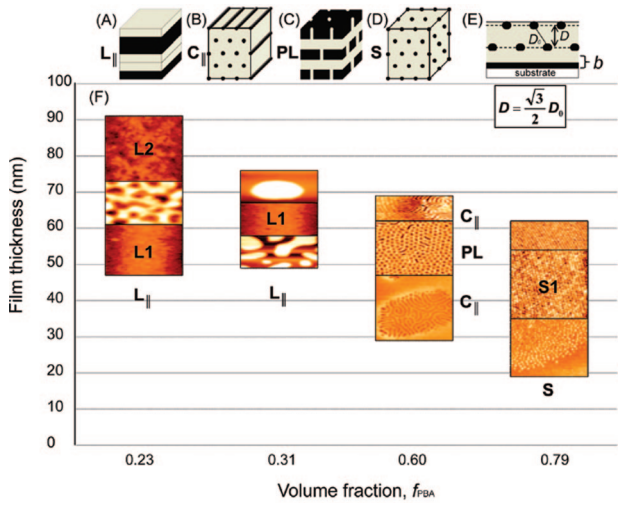

Figure 7. Schematic of (A) lamellae lying parallel to the substrate, $L_{||}$; (B) cylinders lying parallel, $C_{||}$; (C) perforated lamella, PL; (D) spheres, S; (E) half-lamella (brush) formation on top of the silicon substrate in the cylinder and sphere domains. For our system, the black and white phases represent PMMA and PBA blocks, respectively. (F) Summary of results on microphase separation of the considered block copolymer PMMA−PBA in thin annealed films.

cylindrical layer thickness. The mismatch between the period of the perforated lamella and the cylindrical layer thickness was observed previously in thin films of a cylinder-forming system.[69] In this case the measured average island thickness is $D = 48 \pm 5$ nm. This distance layer thickness is compatible with the expected value of 44 ± 1 nm, given by the expression $D = (\sqrt{3}/2)D_0$, derived as in the geometric construction of Figure 7B.

As the film thickness increases to about 60 nm, the hole/island morphology develops again, as shown in Figure 5D and insets, indicating the formation of an incomplete second cylindrical layer ($C_{||,2}$). A perforated PMMA lamella (PL) still occupies the bottom surface. As shown in inset 5D2, on top of the islands PMMA cylinders lay parallel to the substrate within a PBA matrix, indicating that as the film thickness increases again a further transition from the PL domain to a $C_{||}$ domain occurs. A similar domain transition $C_{||} \rightarrow PL \rightarrow C_{||}$ with increasing film thickness has been observed in polystyrene (PS)-*b*-polybutadiene (PB) block copolymer thin films with $f_{PS} = 25.5\%$[26] and in triblock copolymers.[25] The cylinder−cylinder distance (D_0) derived from Figure 5D2 is the same as that measured in Figure 5A,B, indicating the same parallel cylinder arrangement both before and after the $C_{||} \rightarrow PL \rightarrow C_{||}$ transition.

2.2.4. $PMMA_{21}$−PBA_{79}. $PMMA_{21}$−PBA_{79} contains a volume fraction of PBA $f_{PBA} = 0.79$. Figure 6A shows the AFM phase image of $PMMA_{21}$−PBA_{79} film of preannealing thickness $t = 20$ nm. Phase contrast is visible only on top of the islands which are ca. 40 ± 3 nm in thickness. No phase contrast is visible on the bottom surface, indicating a half-lamella (brush) of this PMMA−PBA block copolymer attached to the substrate, similarly to what observed for $PMMA_{40}$−PBA_{60}. Figure 6A2 is a magnified view of the surface of the island in the bottom left.

Considering the volume fraction of PMMA ($f_{PMMA} = 0.21$), we attribute the bright dots within the dark matrix to spheres of PMMA in a matrix of PBA. With increasing film thickness, the area occupied by the islands increases, as expected, with similar phase contrast as in thinner films, as shown in Figure 6B and insets. Figure 6B2 shows hexagonally packed PMMA spheres within a PBA matrix with a regular period of 38 ± 3 nm, as calculated from the regular fast Fourier transform (FFT) images. This hole/island morphology corresponds to an incomplete first layer of PMMA spheres (S1) formed on top of the half-lamella.

For films of preannealing thickness of 43 ± 9 nm, the film becomes an exact multiple of the thickness of the spherical domain layer plus a brush ($D + b$, as depicted in Figure 7E), and the film appears flat throughout. The phase contrast reveals clearly the presence of both blocks near the surface, and no contrast in the topography image can be observed, as shown in Figure 6C1, and the films are remarkably flat. The value of the rms roughness for this film is ca. 0.3 ± 0.1 nm.

At film thickness $t > 54$ nm, a hole/island morphology forms again, as an incomplete second layer of PMMA spheres (S2) forms, as shown in Figure 6D1. Phase contrast is visible on both the top of the islands and on the bottom surface as a hexagonal array of dots, as observed in thinner films. This is confirmation that the spherical domains form a layered structure, similarly to the layered structure observed for the lamellar domains and cylindrical domains.[24,57] The average sphere-to-sphere distance (D_0) calculated from several phase images is 42 ± 6 nm, and the average height of hole/island morphology (D) is 40 ± 3 nm, as expected from the geometrical construction of Figure 7E, where $D = (\sqrt{3}/2)D_0$. Similar layering of sphere domains was recently observed in asymmetric polystyrene (PS)-*b*-poly(2-vinylpyridine) (PVP) diblock copolymer thin films with approximately f_{PVP} of 0.1.[24]

Discussion

The effect of polydispersity on the microphase separation of block copolymers has been studied theoretically for two decades,[31,70−72] but the first experiments have only recently appeared, with the development of synthetic polymerization techniques that allow for sufficient control over molecular weight and composition.[34,73−75] The block copolymers studied here are formed by one monodisperse block (PMMA) and one polydisperse block (PBA). In these copolymers, the Flory−Huggins parameter is low, $\chi N = 12-18$[51] ($\chi_{PMMA/PBA} = 0.03$ at 180 °C and 0.044 at room temperature, based on estimates for monodisperse block copolymers), due to the chemical similarity between the two blocks, so the driving force for the phase separation is not very strong. Yet, calorimetric measurements performed on bulk samples indicated the presence of two separate glass transition temperatures, which is a signature for some degree of microphase separation in bulk. AFM measurements revealed that, notwithstanding the low χN and the relatively high polydispersity index, these block copolymers synthesized by the simple RAFT polymerization show microphase separation with high degree of spatial order, in many respects similar to what expected for highly segregated monodisperse copolymers. By studying the phase separation in thin films of thickness lower than 100 nm, we could investigate the interplay between wetting and microphase separation, which had not been observed before experimentally for these polydispersed block copolymers. In the following, we discuss in detail our experimental observations based on AFM phase and topography images.

As summarized in Figure 7F, the PMMA−PBA blocks microphase separate into lamellae parallel to the substrate for volume fractions of f_{PBA} between 0.23 and 0.31; at a volume fraction of $f_{PBA} = 0.60$, the microphase separation is either one of PMMA cylinders in a PBA matrix or an hexagonally packed perforated lamella depending on film thickness. Finally for a volume fraction of $f_{PBA} = 0.79$, the PMMA blocks separate into spheres in the PBA matrix. The blocks segregated in spheres or in perforated lamellae present a high degree of order, as can be seen in FFT images in Figures 5 and 6. Parallel cylinders have a regular and reproducible domain spacing, but no orientational long-range order.

Our first significant result is that, with respect to the phase diagram of monodisperse block copolymers, the region of lamellar domain is shifted toward an asymmetric composition, i.e., toward $f_{PBA} < 0.3$. In this aspect, our findings confirm recent theoretical expectations which show that polydispersity affects the phase boundaries of block copolymer films by shifting them to different volume fractions with respect to the monodisperse case.[36,70−72,76] This remarkable result was confirmed by neutron reflectivity data. It is possible that this particular domain arrangement is the result of the interplay between microphase separation and wetting, with the air/film and substrate/film interfaces favoring the observed microphase separation of the domains into lamellae.

The progression of the lamellar phase through the phase diagram for nearly constant χN values is asymmetric; in other words, the microphase separation into lamellae is asymmetric around $f_{PBA} = 0.5$, and the lamellar domain does not occur again when $f_{PBA} > 0.7$. The shift of phase boundaries resulting in breaking of the phase diagram symmetry was previously observed in simulations.

The second interesting effect of polydispersity is that a larger range of film thicknesses can accommodate a flat film without displaying hole/island morphologies. This means again that the system comprising chains of variable length is more flexible to adapt to certain morphologies, especially in the case of the lamellar morphology. This was observed in particular for $PMMA_{77}$−PBA_{23} and $PMMA_{69}$−PBA_{31}, in which thin films are flat and uniform and microphase separate in complete parallel lamellae for thickness that are $t = (nL_0 + b) \pm xL_0$ nm, where x can be as high as 0.4−0.5. This observation seems to be consistent with the simulation work by Burger et al. which observed an increase in the area of the stability regions on the phase diagram for copolymers with increased PDI.[31] Also, this observation is compatible with the general impression in simulations that polydispersed copolymers have larger domain spacing as compared to monodisperse systems. The mechanism of the increase of domain spacing is based on the existence of different chain lengths in a system leading to a decrease of the stretching energy.[51,77−79] The presence of a large distribution of chains within the same system seems to allow for greater adaptability and flexibility of polydisperse chains to morphologies which would be metastable or unstable in a monodisperse systems.

Our third important observation is the stabilization of the hexagonally perforated lamella morphology, which is assumed to be metastable in monodisperse copolymers. This result is in agreement with recent simulation work by Matsen,[36] who predicted the formation of a mixed lamellar and cylindrical region due to increased PDI, and work by Listak et al., who observed the formation of an hexagonally perforated lamella on thick solvent cast films.[75] However, in our thin films, the perforated lamellae occur only in certain thickness regimes and for a composition where the polydisperse block is the majority block ($f_{PBA} = 0.6$). As previously suggested, the polydispersity mitigates the chain packing frustration and stabilizes structures with high standard deviation of mean curvature, such as the perforated lamella.

By studying thin films of PMMA−PBA block copolymers, we were able to investigate the interplay between polydispersity and wetting effects. This interplay was particularly evident in copolymers with $f_{PBA} = 0.23$, 0.31, and 0.6. At $f_{PBA} = 0.60$, as depicted in Figure 7F, the perforated lamellae are only stable in a specific thickness regime. At $f_{PBA} = 0.60$, as the film thickness increases, we observe two transitions: the first between parallel cylinders and perforated lamellae and the second back to parallel cylinders. These transitions are likely to be caused by the preference of the system for the structure that presents the least degree of frustration of its characteristic period. As previously observed for thin films of copolymers,[22,27] the frustration of the lamellar period is avoided by changing the orientation of the lamella from parallel to perpendicular to the surface or better by forming a combination of the two morphologies, such as in the perforated lamella. This transition is particularly likely in a system, such as ours, where the two substrate/film and film/air interfaces are almost nonselective toward the two blocks, given their chemical similarity.

Our study confirms that simple synthetic techniques such as RAFT polymerization have the potential to be valid alternatives to more complicated polymerization techniques and can produce block copolymers of well-controlled architecture, polydispersity, and composition. For the first time thin films of RAFT-polymerized block copolymers are shown to be ideal model systems to confirm existing and future simulation results on the interplay between interfacial wetting, microphase separation, and polydispersity in confined geometries.[31,36,72,77] Contrary to what observed for block copolymers synthesized by nitroxide-mediated polymerization,[51] block copolymers made by RAFT with one polydisperse block and with low degree of incompatibility χN microphase separate with high reproducibility and with excellent degree of long-range order. Block copolymers synthesized by RAFT are therefore demonstrated to be valid candidates in numerous advanced materials applications that rely on the formations of ordered patterns, such as suboptical large-scale patterns, photonic materials, and high-density magnetic recording devices.

Conclusions

We studied the phase separation of PMMA−PBA block copolymers synthesized by RAFT polymerization, containing one block with PDI = 1.3−1.4, and spin-cast in films thinner than 100 nm. Thermal characterization of the bulk samples studied by DSC and TGA highlighted the presence of two glass transition temperatures (T_g), which suggests the occurrence of microphase separation in bulk, and showed that the block copolymers are not degraded at a temperature of 180 °C. Annealing of the thin films at 180 °C induced microphase separation of the blocks. As volume fraction f_{PBA} increases from 0.23 to 0.60, the microphase separation changes from lamellar to cylindrical domains and then to spherical at a volume fraction of 0.79. Remarkably, at a volume fraction f_{PBA} of 0.23−0.31 we observe lamellae parallel to the substrate, as predicted in simulations for polydisperse systems. At a PBA volume fraction of 0.6, domain transitions from parallel cylinders to perforated lamellae to parallel cylinders were observed with increasing film thickness. A wetting layer of a half-lamella PMMA−PBA brush is present underneath all films due to the preference of the PMMA block for the substrate.

It was shown that RAFT polymerization produces block copolymers that are suitable for controlled and reproducible studies of microphase separation. These blocks, with a low degree of incompatibility χN, microphase separate into regularly ordered domains and confirm the trends expected from simulations on similar polydisperse block copolymers. The main difference in domain formation with respect to monodisperse systems is the shift of the domain boundaries to more asymmetric volume fractions, the ability to accommodate domains in layers different from exact multiples of a layer period, and the stabilization of hexagonally perforated lamellae.

Supporting Information Available: Neutron reflectivity data. This material is available free of charge via the Internet at http://pubs.acs.org.

References and Notes

(1) Segalman, R. A. *Mater. Sci. Eng. R* **2005**, *48* (6), 191–226.
(2) Darling, S. B. *Prog. Polym. Sci.* **2007**, *32* (10), 1152–1204.
(3) Hamley, I. W. *Nanotechnology* **2003**, *14*, R39−R54.
(4) Bates, F. S.; Fredrickson, G. H. *Phys. Today* **1999**, *52* (2), 32–38.
(5) Bates, F. S.; Fredrickson, G. H. *Annu. Rev. Phys. Chem.* **1990**, *41* (1), 525–557.
(6) Hamley, I. W. *The Physics of Block Copolymers*; Oxford University Press: New York, 1998; p 424.
(7) Menelle, A.; Russell, T. P.; Anastasiadis, S. H.; Satija, S. K.; Majkrzak, C. F. *Phys. Rev. Lett.* **1992**, *68* (1), 67.
(8) Russell, T. P.; Coulon, G.; Deline, V. R.; Miller, D. C. *Macromolecules* **1989**, *22* (12), 4600–4606.
(9) Henkee, C. S.; Thomas, E. L.; Fetters, L. J. *J. Mater. Sci.* **1988**, *23* (5), 1685–1694.
(10) Hashimoto, T.; Tanaka, H.; Hasegawa, H. *Macromolecules* **1990**, *23* (20), 4378–4386.
(11) Vanzo, E. *J. Polym. Sci., Part A: Polym. Chem.* **1966**, *4* (7), 1727–1730.
(12) Bradford, E. B.; Vanzo, E. *J. Polym. Sci., Part A: Polym. Chem.* **1968**, *6* (6), 1661–1670.
(13) Green, P. F.; Limary, R. *Adv. Colloid Interface Sci.* **2001**, *94* (1−3), 53–81.
(14) Tang, C.; Lennon, E. M.; Fredrickson, G. H.; Kramer, E. J.; Hawker, C. J. *Science* **2008**, *322* (5900), 429–432.
(15) Thomas, E. L.; Alward, D. B.; Kinning, D. J.; Martin, D. C.; Handlin, D. L.; Fetters, L. J. *Macromolecules* **1986**, *19*, 2197–2202.
(16) Forster, S.; Khandpur, A. K.; Zhao, J.; Bates, F. S.; Hamley, I. W.; Ryan, A. J.; Bras, W. *Macromolecules* **1994**, *27*, 6922–6935.
(17) Khandpur, A. K.; Farster, J. S.; Bates, F. S.; Hamley, I. W.; Ryan, A. J.; Bras, W.; Almdal, K.; Mortensen, K. *Macromolecules* **1995**, *28*, 8796–8806.
(18) Krausch, G. *Mater. Sci. Eng.* **1995**, *14* (1−2), 1–94.
(19) Coulon, G.; Russell, T. P.; Deline, V. R.; Green, P. F. *Macromolecules* **1989**, *22* (6), 2581–2589.
(20) Anastasiadis, S. H.; Russell, T. P.; Satija, S. K.; Majkrzak, C. F. *Phys. Rev. Lett.* **1989**, *62* (16), 1852.
(21) Collin, B.; Chatenay, D.; Coulon, G.; Ausserre, D.; Gallot, Y. *Macromolecules* **1992**, *25*, 1621–1622.
(22) van Dijk, M. A.; van den Berg, R. *Macromolecules* **1995**, *28* (20), 6773–6778.
(23) Sundrani, D.; Darling, S. B.; Sibener, S. J. *Langmuir* **2004**, *20* (12), 5091–5099.
(24) Yokoyama, H.; Mates, T. E.; Kramer, E. J. *Macromolecules* **2000**, *33* (5), 1888–1898.
(25) Knoll, A.; Magerle, R.; Krausch, G. *J. Chem. Phys.* **2004**, *120* (2), 1105–1116.
(26) Tsarkova, L.; Knoll, A.; Krausch, G.; Magerle, R. *Macromolecules* **2006**, *39* (10), 3608–3615.
(27) Huinink, H. P.; Brokken-Zijp, J. C. M.; van Dijk, M. A.; Sevink, G. J. A. *J. Chem. Phys.* **2000**, *112* (5), 2452–2462.
(28) Lynd, N. A.; Hillmyer, M. A.; Matsen, M. W. *Macromolecules* **2008**, *41*, 4531–4533.
(29) Matsushita, Y.; Noro, A.; Iinuma, M.; Suzuki, J.; Ohtani, H.; Takano, A. *Macromolecules* **2003**, *36*, 8074–8077.
(30) Noro, A.; Iinuma, M.; Suzuki, J.; Takano, A.; Matsushita, M. *Macromolecules* **2004**, *37*, 3804–3808.
(31) Burger, C.; Ruland, W.; Semenov, A. N. *Macromolecules* **1990**, *23* (13), 3339–3346.
(32) Lynd, N. A.; Hamilton, B. D.; Hillmyer, M. A. *J. Polym. Sci., Part B: Polym. Phys.* **2007**, *45* (24), 3386–3393.
(33) Lynd, N. A.; Hillmyer, M. A. *Macromolecules* **2005**, *38*, 8803–8810.
(34) Lynd, N. A.; Hillmyer, M. A. *Macromolecules* **2007**, *40*, 8050–8055.
(35) Matsen, M. W. *J. Chem. Phys.* **1997**, *106* (18), 7781–7791.
(36) Matsen, M. W. *Phys. Rev. Lett.* **2007**, *99* (14), 148304–4.
(37) Baskaran, D.; Muller, A. H. E. *Prog. Polym. Sci.* **2007**, *32* (2), 173–219.
(38) Matyjaszewski, K. *Controlled/Living Radical Polymerisation: From Synthesis to Materials*; American Chemical Society: Washington, DC, 2006.
(39) Matyjaszewski, K.; Davis, T. P. *Handbook of Radical Polymerization*; John Wiley and Sons: Hoboken, 2002.
(40) Chiefari, J.; Chong, Y. K.; Ercole, F.; Krstina, J.; Jeffery, J.; Le, T. P. T.; Mayadunne, R. T. A.; Meijs, G. F.; Moad, C. L.; Moad, G.; Rizzardo, E.; Thang, S. H. *Macromolecules* **1998**, *31* (16), 5559–5562.
(41) Barner-Kowollik, C.; Davis, T. P.; Heuts, J. P. A.; Stenzel, M. H.; Vana, P.; Whittaker, M. *J. Polym. Sci., Polym. Chem.* **2003**, *41* (3), 365–375.
(42) Moad, G.; Rizzardo, E.; Thang, S. H. *Acc. Chem. Res.* **2008**, *41* (9), 1133–1142.
(43) Takolpuckdee, P.; Westwood, J.; Lewis, D. M.; Perrier, S. *Macromol. Symp.* **2004**, *216*, 23–35.
(44) Moad, G.; Rizzardo, E.; Thang, S. H. *Aust. J. Chem.* **2006**, *59* (10), 669–692.
(45) Perrier, S.; Takolpuckdee, P. *J. Polym. Sci., Polym. Chem.* **2005**, *43* (22), 5347–5393.
(46) Tong, J. D.; Jerôme, R. *Polymer* **2000**, *41* (7), 2499–2510.
(47) García, M. F.; de la Fuente, J. L.; Fernández-Sanz, M.; Madruga, E. L. *Polymer* **2001**, *42* (23), 9405–9412.
(48) Buzin, A. I.; Pyda, M.; Costanzo, P.; Matyjaszewski, K.; Wunderlich, B. *Polymer* **2002**, *43* (20), 5563–5569.
(49) Tong, J. D.; Moineau, G.; Leclere, P.; Bredas, J. L.; Lazzaroni, R.; Jerome, R. *Macromolecules* **2000**, *33* (2), 470–479.
(50) Rasmont, A.; Leclère, P.; Doneux, C.; Lambin, G.; Tong, J. D.; Jérôme, R.; Brédas, J. L.; Lazzaroni, R. *Colloids Surf., B* **2000**, *19* (4), 381–395.
(51) Ruzette, A. V.; Tence-Girault, S.; Leibler, L.; Chauvin, F.; Bertin, D.; Guerret, O.; Gerard, P. *Macromolecules* **2006**, *39* (17), 5804–5814.
(52) van der Berg, R.; de Greoot, H.; van Dijk, M. A.; Denley, D. R. *Polymer* **1994**, *35*, 5778–5781.
(53) McLean, R. S.; Sauer, B. B. *Macromolecules* **1997**, *30* (26), 8314–8317.
(54) Magonov, S. N.; Cleveland, J.; Elings, V.; Denley, D.; Whangbo, M. H. *Surf. Sci.* **1997**, *389* (1−3), 201–211.
(55) Magerle, R. *Phys. Rev. Lett.* **2000**, *85* (13), 2749.
(56) Park, I.; Park, S.; Park, H. W.; Chang, T.; Yang, H.; Ryu, C. Y. *Macromolecules* **2006**, *39* (1), 315–318.
(57) Segalman, R. A.; Schaefer, K. E.; Fredrickson, G. H.; Kramer, E. J. *Macromolecules* **2003**, *36*, 4498–4506.
(58) Magonov, S. N.; Reneker, D. H. *Annu. Rev. Mater. Sci.* **1997**, *27* (1), 175.
(59) Thang, S. H.; Chong, Y. K.; Mayadunne, R. T. A.; Moad, G.; Rizzardo, E. *Tetrahedron Lett.* **1999**, *40* (12), 2435–2438.
(60) Neto, C.; Jacobs, K.; Seemann, R.; Blossey, R.; Becker, J.; Grün, G. *J. Phys.: Condens. Matter* **2003**, *15*, 3355–3366.
(61) James, M.; Nelson, A.; Brule, A.; Schulz, J. C. *J. Neutron Res.* **2006**, *14* (2), 91–108.
(62) Nelson, A. *J. Appl. Crystallogr.* **2006**, *39*, 273–276.
(63) Legge, T. M.; Slark, A. T.; Perrier, S. *J. Polym. Sci., Polym. Chem.* **2006**, *44* (24), 6980–6987.
(64) Postma, A.; Davis, T. P.; Li, G.; Moad, G.; O'Shea, M. S. *Macromolecules* **2006**, *39* (16), 5307–5318.
(65) Chong, B.; Moad, G.; Rizzardo, E.; Skidmore, M.; Thang, S. H. *Aust. J. Chem.* **2006**, *59* (10), 755–762.
(66) Wang, H.; Djurisic, A. B.; Chan, W. K.; Xie, M. H. *Appl. Surf. Sci.* **2005**, *252* (4), 1092–1100.
(67) Knoll, A.; Lyakhova, K. S.; Horvat, A.; Krausch, G.; Sevink, G. J. A.; Zvelindovsky, A. V.; Magerle, R. *Nat. Mater.* **2004**, *3* (12), 886–891.
(68) Ludwigs, S.; Boker, A.; Voronov, A.; Rehse, N.; Magerle, R.; Krausch, G. *Nat. Mater.* **2003**, *2* (11), 744–747.
(69) Knoll, A.; Horvat, A.; Lyakhova, K. S.; Krausch, G.; Sevink, G. J. A.; Zvelindovsky, A. V.; Magerle, R. *Phys. Rev. Lett.* **2002**, *89* (3), 035501.
(70) Leibler, L.; Benoit, H. *Polymer* **1981**, *22*, 195–201.
(71) Sides, W.; Fredrickson, G. H. *J. Chem. Phys.* **2004**, *121*, 4974–4986.
(72) Cooke, D. M.; Shi, A.-C. *Macromolecules* **2006**, *39*, 6661–6671.
(73) Bendejacq, D.; Ponsinet, V.; Joanicot, M.; Loo, Y.-L.; Register, R. A. *Macromolecules* **2002**, *35*, 6645–6649.
(74) Ruzette, A.-V.; Tence-Girault, S.; Leibler, L. *Macromolecules* **2006**, *39*, 5804–5814.
(75) Listak, J.; Jakubowski, W.; Mueller, L.; Plichta, A.; Matyjaszewski, K.; Bockstaller, M. R. *Macromolecules* **2008**, *41* (15), 5919–5927.
(76) Matsen, M. W. *Eur. Phys. J. E* **2006**, *21*, 199–207.
(77) Matsen, M. W.; Bates, F. S. *Macromolecules* **1996**, *29* (4), 1091–1098.
(78) Matsen, M. W. *Phys. Rev. Lett.* **2007**, *99* (14), 148304.
(79) Cooke, D. M.; Shi, A. *Macromolecules* **2006**, *39*, 6661–6671.

MA9004428